Journal of Molecular Catalysis A: Chemical 356 (2012) 78–84

Contents lists available at SciVerse ScienceDirect

Journal of Molecular Catalysis A: Chemical

journal homepage: www.elsevier.com/locate/molcata

Cysteine modified anatase TiO_2 hollow microspheres with enhanced visible-light-driven photocatalytic activity

Kangle Lv[a,b,*], Juncheng Hu[a], Xianghong Li[a], Mei Li[a]

[a] Key Laboratory of Catalysis and Materials Science of the State Ethnic Affairs Commission & Ministry of Education, Hubei Province, South-Central University for Nationalities, Wuhan 430074, China

[b] State Key Laboratory of Advanced Technology for Materials Synthesis and Processing, Wuhan University of Technology, Wuhan 430070, China

ARTICLE INFO

Article history:
Received 24 September 2011
Received in revised form
29 December 2011
Accepted 31 December 2011
Available online 8 January 2012

Keywords:
TiO_2 hollow microsphere
Dope
Cysteine
Visible light
Photocatalysis

ABSTRACT

Preparation of visible-light responsive TiO_2 photocatalyst for recycling and repeated use is of great importance in practical application, such as water purification. In this paper, anatase TiO_2 hollow microspheres were prepared using $Ti(SO_4)_2$ and NH_4F as the starting materials, which were then mixed with cysteine, a biomolecule, followed by calcination at 300 °C for 2 h. The cysteine modified TiO_2 hollow microspheres were characterized by X-ray diffraction, scanning electron microscopy, transmission electron microscopy, nitrogen adsorption–desorption isotherms, UV–vis diffuse reflectance spectra, X-ray photoelectron spectroscopy, photoluminescence and photocurrent. The photocatalytic activity of cysteine modified TiO_2 hollow microspheres was evaluated using Brilliant Red X3B, an anionic azo dye, as the target organic molecule under visible light irradiation ($\lambda \geq 400$ nm). The experimental results showed that C, N and S elements were doped into the lattices of TiO_2 hollow microspheres, resulting in an obvious increase in visible-light harvesting ability. With increase in the molar ratio of cysteine to titania (R) from 0 to 2.0, the visible-light photocatalytic activity of the samples increase first, and then decrease. The photocatalyst with $R = 1.0$ shows the highest photocatalytic activity, which is 6 and 4 times higher than that of pristine TiO_2 counterpart and commercial P25 photocatalyst, respectively. The enhanced photocatalytic activity of cysteine modified TiO_2 hollow microspheres is attributed to the synergistic effects of improved visible-light harvesting ability, enhanced adsorption to organic pollutant and increased efficiency in separation of the photo-generated electron and hole.

1. Introduction

In recent years, anatase TiO_2 hollow nanostructures have received considerable attention due to their high surface-to-volume ratios, lower density, better permeation and wide potential applications in solar energy conversion and environmental purification such as water disinfection, hazardous waste remediation and air purification [1–7]. Up to now, most of the approaches for hollow structures rely on the use of sacrificial templates (either hard or soft). One-pot template-free methods for hollow structures was also developed based on direct solid evacuation with Ostwald ripening and the Kirkendall effect [8]. Recently, hollow anatase-phase TiO_2 microspheres with mesoporous shells were fabricated on a large scale by fluoride-induced self transformation [9]. Compared with that of nanoparticles, the photocatalytic activity of anatase TiO_2 hollow microspheres was enhanced, possibly due to multiple reflections of UV light within the sphere interior voids [10]. Anatase TiO_2 hollow microspheres have the advantage of recycling and repeated use [11,12]. They, however, can still only be activated by UV light (band gap 3.2 eV). Therefore, visible-light-driven anatase TiO_2 hollow microspheres are highly desired.

Doping TiO_2 with metal or nonmetal atoms is an effective way to convert the TiO_2 absorption from the ultraviolet to the visible region [13–15]. Our previous study showed that compared with Bi doped TiO_2 nanoparticles, Bi, C and N co-doped TiO_2 nanoparticles showed higher photoreactivity whatever under visible or UV light irradiation, reflecting the synergistic effect of different dopant on the enhanced photocatalytic activity of TiO_2 [14]. Yu et al. found that the band gap of N,S-codoped TiO_2 powders were narrowed by mixing the N 2p and S 3p states with O 2p states [16]. Among nonmetal dopants, C [17–19], N [4,20–25] and S [16,26] are the most efficient. But it is challenging yet desirable to incorporate dopants into anatase TiO_2 hollow microspheres, especially for these prepared by fluoride induced self-transformation. This is because anatase TiO_2 hollow microspheres usually have very high

* Corresponding author at: Key Laboratory of Catalysis and Materials Science of the State Ethnic Affairs Commission & Ministry of Education, Hubei Province, South-Central University for Nationalities, Wuhan 430074, China. Tel.: +86 27 67842752; fax: +86 27 67842752.
E-mail address: lvkangle@mail.scuec.edu.cn (K. Lv).

1381-1169/$ – see front matter © 2012 Elsevier B.V. All rights reserved.
doi:10.1016/j.molcata.2011.12.028

Table 1
Characterization results and the adsorption of X3B.

Catalyst	Phase content[a]	Crystalline size[b] (nm)	Surface area[c] (m^2/g)	Pore volume[d] (cm^3/g)	Average pore size (nm)	n_{ad}[e] (μmol/g)
R0	A	16.6	45.1	0.22	18.1	15.9
R0.5	A	15.3	46.1	0.21	16.3	29.9
R0.75	A	14.9	47.0	0.21	15.3	38.6
R1.0	A	15.1	53.4	0.17	13.0	40.9
R1.5	A	14.1	66.2	0.18	11.2	60.1
R2.0	A	13.7	78.1	0.18	9.2	73.7
P25	A:R = 8:2	24.5	45.0	0.15	13.6	19.7

[a] A and R denote anatase and rutile, respectively.
[b] Average anatase crystalline size of TiO_2 was determined by XRD using Scherrer equation.
[c] The BET surface area was determined by a multipoint BET method using the adsorption data in P/P_0 range from 0.05 to 0.25.
[d] Pore volume and average pore size were determined by nitrogen adsorption volume at $P/P_0 = 0.994$.
[e] n_{ad} was the amount of dye adsorbed before irradiation.

crystallinity, making it hard or nearly impossible to incorporate dopants into them by mild post-treatment, while the addition of dopant precursors in the reaction medium may inevitably influence the nucleation and growth of anatase TiO_2 hollow microspheres so that no desirable visible-light-driven anatase TiO_2 hollow microspheres were synthesized.

In this paper, visible-light-driven C, N and S tri-doped TiO_2 hollow microspheres were prepared using L-cysteine (HS—CH(NH_2)—COOH, CAS No. 52-90-4), a biomolecule, as modified reagent. The aim of the paper is to study the synergistic effect of different nonmetal co-doping on the photocatalytic activity of TiO_2 hollow microspheres by cysteine modification. It is proposed that the optical properties and therefore the photocatalytic activity of TiO_2 can be further tailored by doping C, N and S elements at the same time when compared with by doping with only one or two elements. To the best of our knowledge, it is the first example to report the visible-light-driven anatase TiO_2 hollow microspheres by doping three nonmetal elements at the same time using a biomolecule as modified reagent. Compared with the method of doping TiO_2 through hydrothermal reaction [18], this method is more simple, cost-effective, and environmental friendly. The dramatic enhancement in photocatalytic activity under visible light were explained on the basis of the synergetic effects of promoted visible light harvesting ability, enhanced adsorption of the dye and improved efficiency on separation of photo-generated carriers.

2. Experimental

2.1. Preparation

Hollow TiO_2 microspheres were prepared by fluoride-induced self transformation [9,11]. Briefly, 1.2 g of $Ti(SO_4)_2$ (5.0 mmol) and 0.185 g of NH_4F (5.0 mmol) were dissolved in 75 mL doubly distilled water under vigorous magnetic stirring. Then, 0.6 g of urea (10.0 mmol) was added. The resulted transparent solution was transferred to a 100-mL Teflon-lined autoclave. The autoclave was sealed and kept at 200 °C for 24 h. After being cooled to room temperature, the white precipitates were filtrated through a membrane filter (pore size, 0.45 μm), and thoroughly rinsed with distilled water until the pH of the filtrate is about 7. The precipitates were then dried in a vacuum oven at 80 °C for 10 h.

The typical preparation of visible-light-driven cysteine modified TiO_2 hollow microspheres was as follows: Firstly, 0.2 g of the as-prepared anatase TiO_2 hollow microspheres was added into a beaker which contained 5 mL of L-cysteine (Shanghai Chemical Inc.) solution. After an ultrasonic bath for 10 min to make cysteine totally disperse, the mixed solution was dried in oven at 80 °C. Secondly, the dried opaque powder was ground and calcined at 300 °C for 2 h in a furnace. According to this method, different mass ratio of cysteine to titanium (R) photocatalysts from 0 to 2.0 were synthesized. For simplification, the prepared TiO_2 samples are denoted as R. R0 refers to the undoped pristine TiO_2 sample (Table 1).

2.2. Characterization

The X-ray diffraction (XRD) patterns obtained on a D8- advance X-ray diffractometer (German Bruker) using Cu Kα radiation at a scan rate of 0.02° $2\theta\,s^{-1}$ were used to determine the crystalline size and identity. The accelerated voltage and applied current were 15 kV and 20 mA, respectively. The average crystalline size of the catalyst was determined according to the Scherrer equation using full width at half maximum (FWHM) data after correcting for the instrumental broadening. The transmission electron microscopy (TEM) images were obtained by Tecnai G20 transmission electron microscope operated at an accelerating voltage of 200 kV, and the scanning electron microscopy (SEM) images were obtained by a field emission scanning electron microscope (Hitach, Japan) with an acceleration voltage of 5 kV. The BET surface area (S_{BET}) of the powders was analyzed by using nitrogen adsorption in a nitrogen-adsorption apparatus (Micromeritics ASAP 2020, USA). All the samples were degassed at 180 °C prior to the nitrogen-adsorption measurements. UV–vis diffuse reflectance spectroscopy (DRS) was carried out on a Hitachi U-3010 UV–vis spectrophotometer. $BaSO_4$ was the reference sample. UV–visible absorbance spectra were obtained for the dry-pressed disk samples with a UV–Visible spectrophotometer (UV-2550, Shimadzu, Japan). $BaSO_4$ was used as a reflectance standard in a UV–visible diffuse reflectance experiment. X-ray photoelectron spectroscopy (XPS) measurements were performed with a Multilab 2000 XPS system with a monochromatic Mg Kα source and a charge neutralizer. All of the binding energies were referenced to the C 1s peak at 284.4 eV of the surface adventitious carbon. Photoluminescence (PL) spectra were measured at room temperature on a Fluorescence Spectrophotometer (F-7000, Hitachi, Japan). The excitation wavelength was 315 nm, the scanning speed was 1200 nm/min, and the PMT voltage was 700 V. The width of excitation slit and emission slit were both 5.0 nm.

2.3. Photocatalytic degradation

A 300 W Xe arc lamp, which produces light spectra similar to that of solar radiation, equipped with an ultraviolet cutoff filter to provide visible light with $\lambda \geq 400$ nm served as the visible light source. Reactive Brilliant Red X3B (X3B, Fig. 1) [27], an anionic organic dye, was used as the target organic pollutant. During the photocatalytic reaction, the reactor was maintained at room temperature through a water recycle system, and was mechanically stirred at a constant rate. The concentration of TiO_2 was 1.0 g/L, and the initial concentration of X3B was 1.0×10^{-4} mol/L. Before irradiation, the solution was sonicated first for 5 min, and then the solution was continuously stirred for about 1 h to ensure the establishment of an adsorption–desorption equilibrium. At given

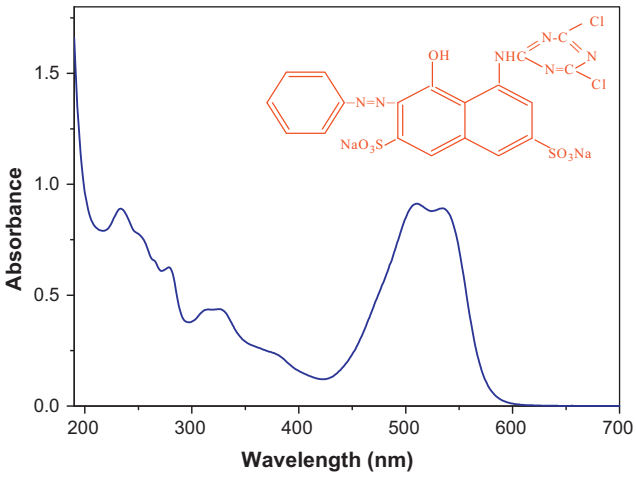

Fig. 1. Structure and electronic absorption spectrum of X3B in water.

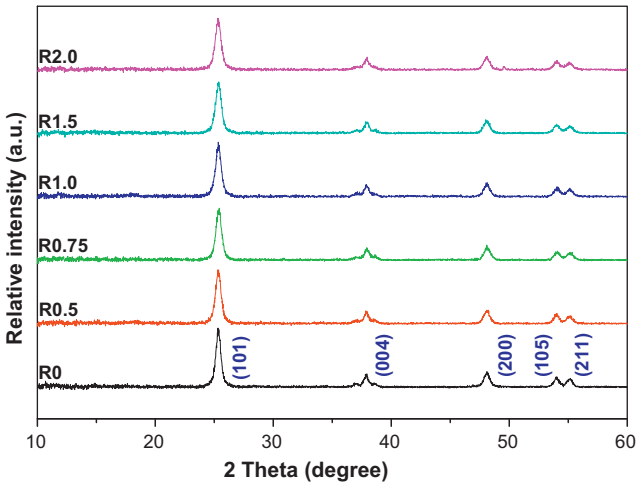

Fig. 2. XRD patterns of the photocatalysts.

intervals of irradiation, small aliquots were withdrawn by a syringe, and filtered through a membrane (pore size 0.45 μm). The concentration of X3B remaining in the filtrate was then analyzed by an Hitachi U-3010 spectrometer at 510 nm.

2.4. Photoelectrochemical measurements

The photoelectric performances were measured on an electrochemical system (CHI-660B, China). A collimated light beam from the xenon lamp with an ultraviolet cutoff filter ($\lambda \geq 400$ nm) was used for excitation of the ITO/TiO_2 electrode. The photoresponses of the photocatalysts as visible light on and off were measured at 0.0 V. To investigate the transition of photogenerated electrons, TiO_2 electrodes were prepared as follows: 5 mg of as-prepared photocatalyst was suspended in 5 mL ethanol to produce slurry, which was then dip-coated onto a 2 cm × 4 cm indium-tin oxide (ITO) glass electrode. The ITO/TiO_2 electrode, Pt plate, and Ag/AgCl electrode were used as the working, counter, and reference electrodes, respectively. 1.0 mol/L KOH solution was used as electrolyte solution. The thickness of the investigated electrodes was about 1 μm.

3. Result and discussion

3.1. Phase structures and morphology

XRD was used to investigate the phase structure of the as-prepared cysteine modified TiO_2 hollow microspheres. Fig. 2 shows the effects of *R* on the phase structures of the TiO_2 powders. All diffraction peaks of the calcined powders were indexed to pure anatase phase of TiO_2 (JPCDS Card: 86-1157, space group: $I4_1/amd$) [15,28]. It can be seen that the *R* slightly influences the crystallization of the TiO_2 powders. With increasing *R*, the FWHM of the anatase peaks are slightly broadened. Such a FWHM broadening suggests a decrease in the size for anatase crystallite (Table 1). This is due to the presence of cysteine which prevents the growth of nanocrystals by inhibiting the extension of Ti—O—Ti bridging.

The morphology of cysteine modified TiO_2 hollow microspheres was studied by SEM and TEM. Fig. 3A shows the SEM image of R1.0 cysteine modified TiO_2 hollow microspheres, from which hollow microspheres consisted of loosely packed nanoparticles could be clearly observed. Fig. 3B shows a typical TEM image of R1.0. The contrast between the dark edges and plate centers further confirms the hollow structure of TiO_2 microspheres. Fig. 3C shows the corresponding high resolution TEM image of R1.0. It shows clear lattice fringes, which allowed for the identification of crystallographic spacing. The fringe spacing of ca. 0.35 nm matches that of the (1 0 1) crystallographic plane of anatase TiO_2 [25].

3.2. BET surface areas and pore size distributions

The porous structures and BET surface areas of as-prepared TiO_2 samples were investigated based on the nitrogen sorption measurement. Fig. 4 shows the nitrogen sorption isotherms and the corresponding pore size distribution curves of R0, R1.0 and R2.0 samples. As for pure TiO_2 hollow microspheres (R0), it can be seen that the isotherm is of types IV (BDDT classification). At high-relative pressure range from 0.7 to 1.0, the isotherm exhibits a hysteresis loop of type H2 associated with the ink bottle pores, indicating that the powders contain mesopores (2–50 nm) [7,11,29]. The corresponding pore size distribution curve of R0 exhibits a

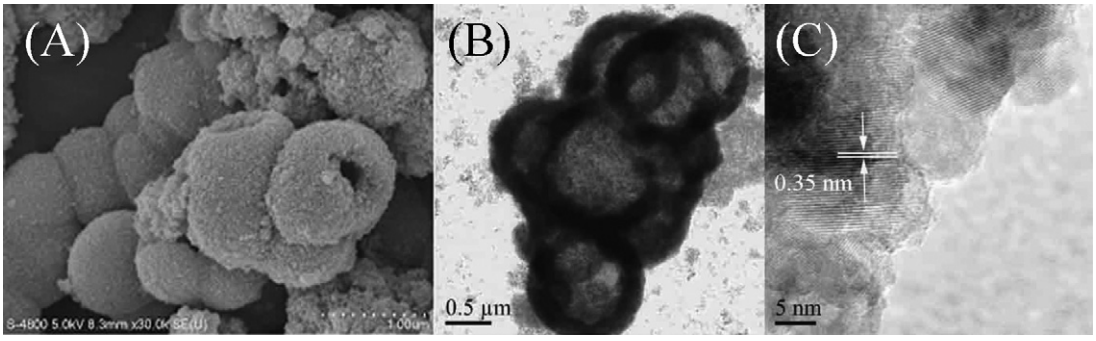

Fig. 3. SEM (A) and TEM (B and C) images of R1.0 TiO_2 sample.

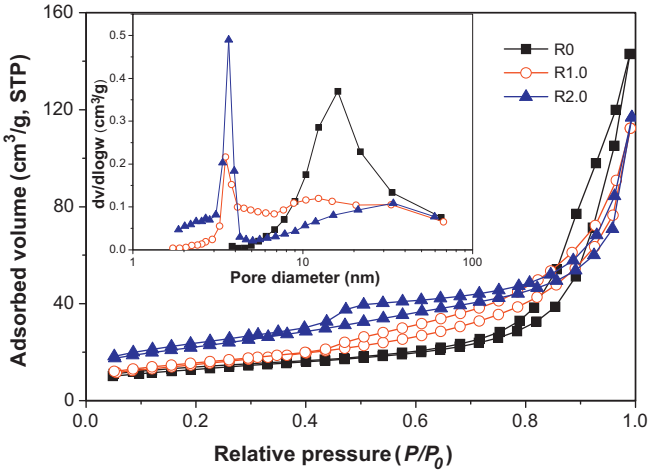

Fig. 4. Nitrogen adsorption–desorption isotherms and the corresponding pore size distributions (inset) of the photocatalysts.

wide pore size distribution with the average pore diameters about 18.1 nm.

With increasing *R*, the adsorption isotherms of the photocatalysts shift upward and the hysteresis loops begin at lower relative pressures (Fig. 4), indicating the increase in the BET specific surface areas and decrease in average pore sizes [30]. This is consistent with the XRD results, ascribed to the presence of cysteine prevents the growth of anatase TiO_2 nanocrystals.

Table 1 shows the effects of *R* on the physical properties of the hollow TiO_2 microspheres. It can be seen that, with increasing *R* from 0 to 2.0, the BET surface area increases from 45.1 to 78.1 m^2/g, while the average pore size decreases from 18.1 to 9.2 cm^3/g. This is due to the decrease in the crystallite sizes of the cysteine modified TiO_2 hollow microspheres.

3.3. XPS analysis

X-ray photoelectron spectroscopy (XPS) measurements are performed to further elucidate the interaction between cysteine and TiO_2. Fig. 5 shows the XPS survey spectra of R0, R1.0 and R2.0 hollow TiO_2 microspheres. It can be seen that R0 sample not only contains Ti, O and C elements, with sharp photoelectron peaks appearing at binding energies of 459 (Ti 2p), 530 (O 1s) and 285 eV (C 1s), but also contain small amount of N, S and F elements with binding

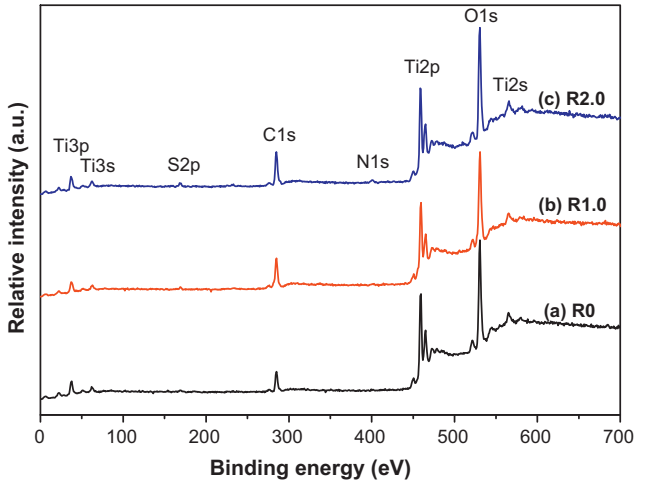

Fig. 5. XPS survey spectra of the hollow TiO_2 microspheres of (a) R0, (b) R1.0 and (c) R2.0, respectively.

Table 2
Composition (at.%) of the photocatalysts prepared before (R0) and after doped with cysteine (R1.0 and R2.0).

Photocatalyst	Composition (at.%)					
	O	Ti	C	F	N	S
R0	50.54	26.64	20.77	0.59	0.73	0.73
R1.0	43.90	21.60	32.01	0.47	1.18	0.84
R2.0	45.17	22.09	28.93	0.39	2.20	1.22

energies of 401 (N 1s), 169 (S 2p) and 685 eV (F 1s), respectively [31]. The composition of the photocatalysts are listed in Table 2, from which it can be seen that the atomic ratio of Ti to O of R0 is about 2, in good agreement with the nominal atomic composition of TiO_2. The peaks of nitrogen, sulfur and fluorine probably come from the starting materials of $Ti(SO_4)_2$ and NH_4F. The carbon peak for R0 sample is attributed to adventitious hydrocarbon from XPS instrument itself, because the starting materials do not contain carbon element [32].

For comparison, the high-resolution XPS spectra of C 1s region of R0 and R1.0 samples are obtained (Fig. 6A and B). It can be seen that the C 1s region of R0 can be deconvoluted into two peaks. The main peak binding energy at about 285.0 eV corresponds to carbons of saturated hydrocarbon groups (at. 95.9%), and the small peak with a binding energy of 289.3 eV comes from oxidized carbon species (at. 4.1%) [18]. On the contrary, the C 1s region of doped R1.0 sample can be deconvoluted into 3 peaks. Besides the 2 peaks mentioned above, an obvious peak with a binding energy of 282.1 eV was deconvoluted, which is ascribed to Ti–C bonds (at. 3.9%) [32].

Fig. 6C shows the corresponding high-resolution XPS spectra of the N 1s region taken from R1.0 sample. The curve of the N 1s region of R1.0 can be deconvoluted into three peaks. The small peak (399.2 eV) is attributed to the Ti–N (at. 18.7%). The other two peaks at about 400.4 and 401.8 eV are assigned to NH_3 (at. 10.7%) and NH_4^+ (at. 70.6%) adsorbed on the surface of TiO_2, respectively [23,24,32].

Fig. 6D shows the high-resolution XPS spectrum of the S 2p region for R1.0 sample. It can be seen that the peak of S 2p contains three isolated peaks at binding energies of 169.1, 166.1 and 164.9 eV, which can be attributed to the S(+VI), organic S(−II) and Ti—S, respectively. The S(+VI) is assigned to the SO_4^{2-} ions adsorbed on the surface of TiO_2 sample, organic S(−II) comes from the cysteine (C—S). The peak at 164.9 eV corresponds to the Ti–S bond due to the fact that S atoms replace O atoms in the TiO_2 lattice [23,26,32].

As expected, an additional peak at 684.6 eV (F 1s) is found in the survey spectrum of R1.0 sample (not shown here) [31].

$$\equiv \mathrm{Ti{-}OH} + \mathrm{HF} \rightarrow \equiv \mathrm{Ti{-}F} + \mathrm{H_2O} \quad (1)$$

The F 1s binding energy peak originates from surface fluoride (≡Ti—F) formed by ligand exchange between F^- and surface hydroxyl groups (Eq. (1)) [33–35]. No signal for F^- in the lattice of TiO_2 (binding energy of 688.5 eV) is found in all the photocatalysts [7,36,37].

According to the above XPS results, it can be concluded that C, N and S elements were in situ doped into the lattice of R1.0 hollow microspheres during calcination. The composition of the detected elements by XPS for R0, R1.0 and R2.0 samples are listed in Table 2. It shows that the content of the N and S elements increases, while F element decreases with increasing *R*. However, the content of carbon does increase with increase in *R*. This is due to the interference of adventitious hydrocarbon from XPS instrument itself. For all the samples, the atomic ratio of Ti to O is about 2, in good agreement with the nominal atomic composition of TiO_2.

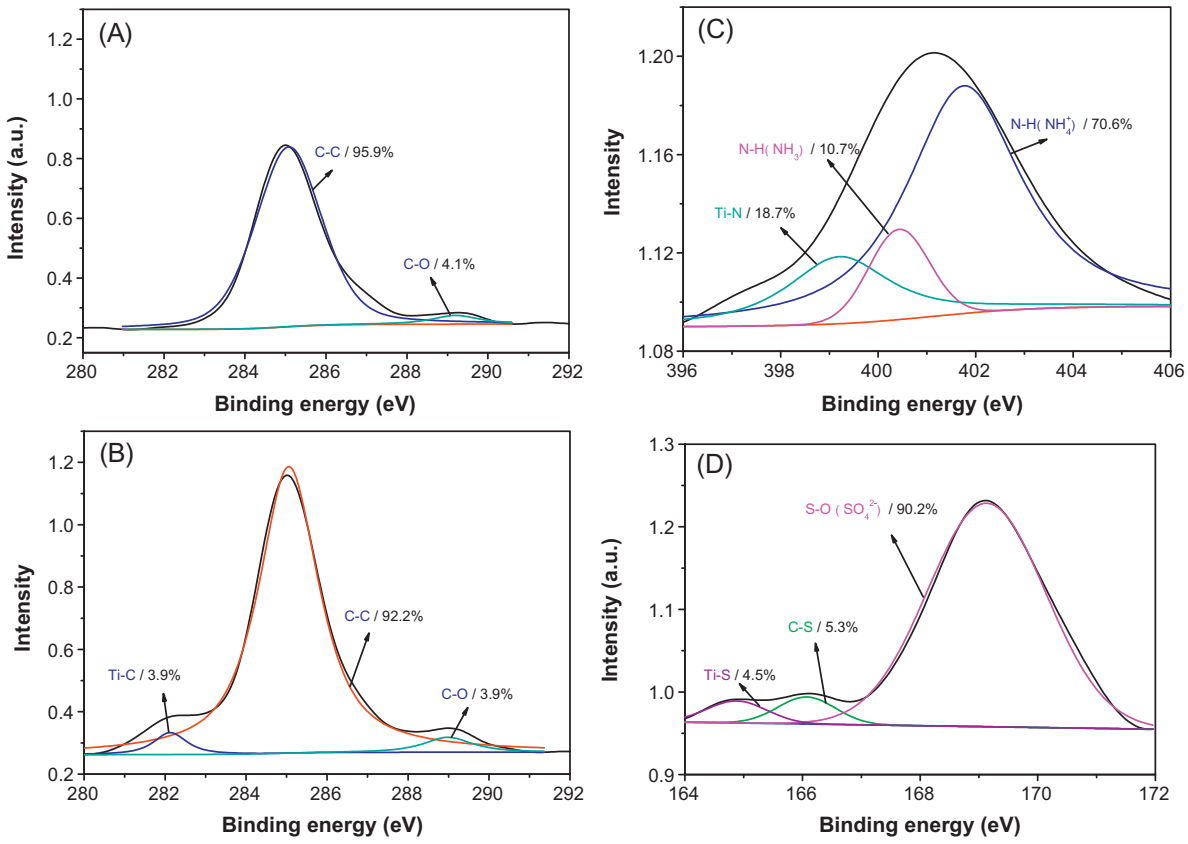

Fig. 6. High-resolution XPS spectra for the C 1s region of R0 (A), C 1s (B), N 1s (C) and S 2p (D) of R1.0 photocatalyst, respectively.

3.4. UV–vis analysis

Usually, doping obviously influences light absorption characteristics of TiO_2 [24]. Therefore, the optical property of the undoped and doped hollow TiO_2 microspheres were measured by UV–vis diffuse reflectance spectra. As displayed in Fig. 7, all of these samples display the typical absorption with an intense transition in the UV region of the spectra, which is assigned to the intrinsic band gap absorption of TiO_2 due to the electron transitions from the valence band to conduction band ($O_{2p} \rightarrow Ti_{3d}$). The pure TiO_2 (R0) shows no absorption above its fundamental absorption edge (around 400 nm). In contrast, the absorption spectra of the cysteine modified TiO_2 samples show a enhanced absorption in the visible light region. Undoubtedly, these results reveal that the nonmetal elements are indeed incorporated into the lattice of TiO_2, forming two phase structures (doped and un-doped anatase TiO_2).

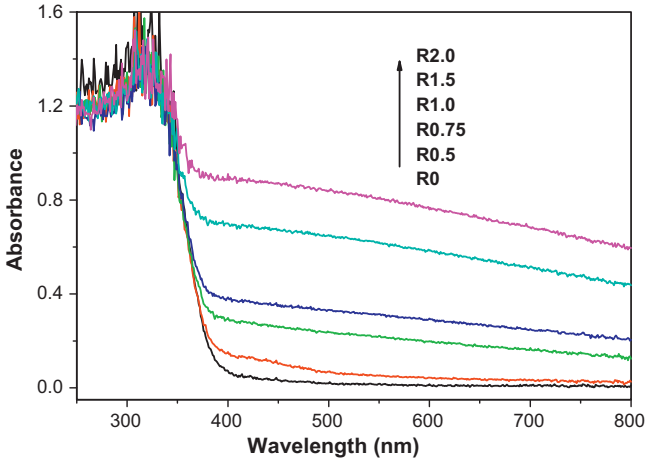

Fig. 7. UV–vis diffuse reflectance spectra of the photocatalyts.

3.5. Adsorption and photocatalytic activity

Photocatalytic activity tests were investigated by the degradation of X3B in aqueous solution under visible light irradiation ($\lambda \geq 400$ nm). It was accepted that adsorption of the organic pollutant on the surface of TiO_2 plays an important role on the photocatalytic degradation [12,27,38]. Here the adsorption of X3B on the surface of the photocatalyst was evaluated before irradiation, and the results were listed in Table 1. It can be seen that the adsorption of X3B on the surface of TiO_2 hollow microspheres increases with increasing *R*. When *R* increases from 0 to 2.0, the amount of X3B adsorbed on the surface of TiO_2 is found to increase from 15.9 to 73.7 μmol/g. Two reasons are responsible for the improved adsorption of the dye. The first is due to the increase in BET specific surface areas of the photocatalysts (Table 1). The second is ascribed to carbonaceous species embed in the TiO_2 matrix, which may lead to the formation of new adsorptive sites [18]. The enhancement on the adsorption of the dye by cysteine modification should also benefit the photocatalytic degradation of X3B.

Fig. 8A shows the degradation profiles of X3B in different conditions. It can be seen that the self-degradation of X3B is negligible, indicating the stabilization of X3B under visible light irradiation. However, in the presence of the TiO_2 photocatalysts, X3B shows obvious degradation. The degradation of X3B on undoped TiO_2 under visible light irradiation can be attributed to the self-sensitization of the dye. The kinetic data for the degradation of X3B can be well fitted by the apparent first-order rate equation, $\ln(C/C_0) = k_{app}t$, where k_{app} is rate constant, C and C_0 are the total

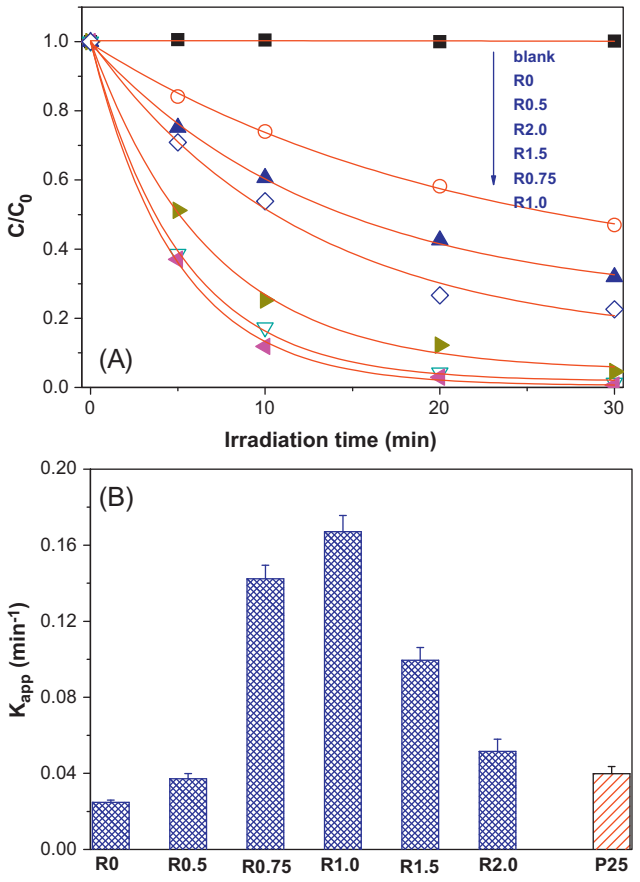

Fig. 8. Dependence of the concentration of X3B on UV irradiation time (A) and comparison of the apparent rate constants (B).

concentration of X3B at irradiation time $t = 0$ and t, respectively. Fig. 8B shows the effect of R on the degradation rate constant of X3B. It can be clearly seen that the photocatalytic activity of TiO_2 hollow microspheres firstly increases and then decreases with increasing R. Sample of R1.0 shows the highest photocatalytic activity (0.17 min^{-1}), which is 4.3, 6.8 and 3.3 times higher than that of P25 (0.04 min^{-1}), undoped R0 (0.025 min^{-1}) and cysteine modified TiO_2 hollow microspheres of R2.0 (0.052 min^{-1}), respectively. This indicates the prepared cysteine modified TiO_2 hollow microspheres is an effective visible-light-driven photocatalyst.

3.6. Reasons for the enhancement of the visible-light driven photoactivity

It was reported that doped TiO_2 powder consists of two phases (un-doped and doped TiO_2) [32]. Usually, the composite of two kinds of semiconductors or two phases of the same semiconductor is beneficial in reducing the recombination of photo-generated electrons and holes and thus enhances photocatalytic activity [30,39,40].

Photoluminescence (PL) analysis is commonly used to analyze the recombination rate of photo-generated electron-hole of TiO_2. Herein, we conduct PL measurement for the pristine (R0) and cysteine modified TiO_2 sample (R1.0 and R2.0), respectively. It can be seen that the emission spectra shapes of R0 and R1.0 are similar and there are five main peaks (Fig. 9). The strong peak at about 397 nm is attributed to the emission of band gap transition, and the other four small peaks, ranging from 440 to 500 nm, are attributed to surface oxygen vacancies and defects [41]. When compared with pure TiO_2 (R0), the intensity of PL signal for R1.0 is much lower.

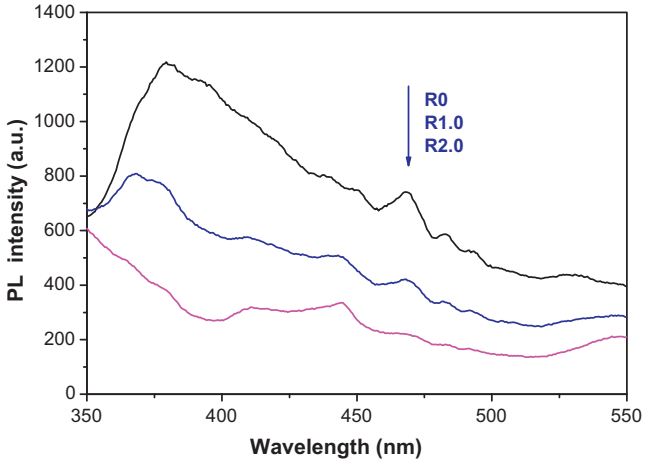

Fig. 9. PL spectra of the samples.

This is due to the reduction of the radiative recombination process, that is, the lower the recombination, the weaker the PL signals are. So, it is understandable that cysteine modified R1.0 shows superior photocatalytic activity than pure TiO_2 (R0).

However, the PL signal peak at about 397 nm is negligible for R2.0 sample. This is due to the light filter effect or PL quenching effect by surface carbon species. Most of the light are adsorbed by surface carbon species (Fig. 7), and some of the generated photoluminescence can also be absorbed by surface carbon species when TiO_2 hollow spheres is modified large amount of cysteine. Therefore, R2.0 shows lower photocatalytic activity than R1.0 sample.

The value of photocurrent can indirectly reflect the semiconductor's ability of generating and transferring of photo-generated charge carriers under irradiation [40,42]. The photocurrent response of three typical TiO_2 samples (R0, R1.0 and R2.0) was further tested in several on–off cycles (Fig. 10). A prompt generation of photocurrents are observed and with good reproducibility when the ITO/TiO_2 electrodes are illuminated. While the lamp is off, the value of photocurrent for all the ITO/TiO_2 samples are instantaneously close to zero. It can be clearly seen that the photocurrent value increases as follows: R0 < R2.0 < R1.0. The photocatalytic activity of TiO_2 is highly related to the number of the separated photo-generated charge carriers [40]. So it can be deduced that the photocatalytic activity of R1.0 is higher than that of R2.0 and R0.

Therefore, improved visible-light harvesting ability by tri-doping of C, N and S elements, enhanced adsorption to the dye X3B;

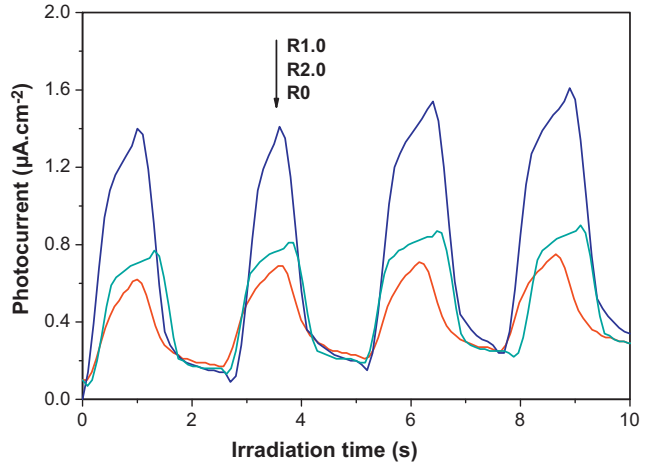

Fig. 10. Photocurrent response of the photocatalysts.

and increased efficiency in separation of photo-generated charge carriers are responsible for the high visible-light-driven cysteine modified TiO_2 hollow microspheres.

Compared with the method of doping TiO_2 through hydrothermal reaction [18], this technique is more convenient and time-saving. The as-prepared cysteine modified TiO_2 hollow microspheres are deemed as potential good candidates for practical application due to their nontoxicity, low processing cost and easy reclamation.

4. Conclusions

Cysteine modified TiO_2 hybride hollow microspheres were successfully fabricated. The high visible-light-driven photocatalytic activity of cysteine modified TiO_2 hollow microspheres is ascribed to the synergetic effects of (1) improved visible-light harvesting ability (doping of C, N and S elements), (2) enhanced adsorption to the dye X3B; and (3) increased efficiency in separation of photo-generated charge carriers. The as-prepared cysteine modified TiO_2 hybride hollow microspheres should find wide-ranging potential applications in various fields including photocatalysis, catalysis, electrochemistry, separation, purification and so on.

Acknowledgements

This work was supported by the National Natural Science Foundation of China (20977114), Natural Science Foundation of Hubei Province (2011CDA107) and China Postdoctoral Science Foundation (201003500).

References

[1] X.W. Lou, L.A. Archer, Z.C. Yang, Adv. Mater. 20 (2008) 3987–4019.
[2] X.X. Li, Y.J. Xiong, Z.Q. Li, Y. Xie, Inorg. Chem. 45 (2006) 3493–3495.
[3] B. Xue, R. Liu, Z.D. Xu, Mater. Lett. 63 (2009) 2377–2380.
[4] Y.M. Wu, M.Y. Xing, B.Z. Tian, J.L. Zhang, F. Chen, Chem. Eng. J. 162 (2010) 710–717.
[5] Y. Zheng, K.L. Lv, X.F. Li, K.J. Deng, J. Sun, L.Q. Chen, L.Z. Cui, D.Y. Du, Chem. Eng. Technol. 34 (2011) 1630–1634.
[6] K.L. Lv, Q.J. Xiang, J.G. Yu, Appl. Catal. B 104 (2011) 275–281.
[7] Z.Y. Wang, K.L. Lv, G.H. Wang, K.J. Deng, D.G. Tang, Appl. Catal. B 100 (2010) 378–385.
[8] K.L. Lv, J.G. Yu, J.J. Fan, M. Jaroniec, CrystEngComm 14 (2011) 7044–7048.
[9] J.G. Yu, S.W. Liu, H.G. Yu, J. Catal. 249 (2007) 59–66.
[10] H.X. Li, Z.F. Bian, J. Zhu, D.Q. Zhang, G.S. Li, Y.N. Huo, H. Li, Y.F. Lu, J. Am. Chem. Soc. 129 (2007) 8406–8407.
[11] J.G. Yu, H.T. Guo, S. Davis, S. Mann, Adv. Funct. Mater. 16 (2006) 2035–2041.
[12] X.F. Li, K.L. Lv, K.J. Deng, J.F. Tang, R. Su, J. Sun, L.Q. Chen, Mater. Sci. Eng. B 158 (2009) 40–47.
[13] X.B. Chen, S.H. Shen, L.J. Guo, S.S. Mao, Chem. Rev. 110 (2010) 6503–6570.
[14] K.L. Lv, H.S. Zuo, J. Sun, K.J. Deng, S.C. Liu, X.F. Li, D.Y. Wang, J. Hazard. Mater. 161 (2009) 396–401.
[15] H.S. Zuo, J. Sun, K.J. Deng, R. Su, F.Y. Wei, D.Y. Wang, Chem. Eng. Technol. 30 (2007) 577–582.
[16] J.G. Yu, M.H. Zhou, B. Cheng, X.J. Zhao, J. Mol. Catal. A 246 (2006) 176–184.
[17] S.U.M. Khan, M. Al-Shahry, W.B. Ingler Jr., Science 297 (2002) 2243–2245.
[18] W.J. Ren, Z.H. Ai, F.L. Jia, L.Z. Zhang, X.X. Fan, Z.G. Zou, Appl. Catal. B 69 (2007) 138–144.
[19] S. Sakthivel, H. Kisch, Angew. Chem. Int. Ed. 42 (2003) 4908–4911.
[20] F. Asahi, T. Morikawa, T. Ohwaki, K. Aoki, Y. Taga, Science 293 (2001) 269–271.
[21] G.H. Tian, H.G. Fu, L.Q. Jing, C.G. Tian, J. Hazard. Mater. 161 (2009) 1122–1130.
[22] B. Naik, K.M. Parida, C.S. Gopinath, J. Phys. Chem. C 114 (2010) 19473–19482.
[23] P. Periyat, D.E. McCormack, S.J. Hinder, S.C. Pillai, J. Phys. Chem. C 113 (2009) 3246–3253.
[24] G. Liu, H.G. Yang, X.W. Wang, L. Cheng, J. Pan, G.Q. Lu, H.M. Cheng, J. Am. Chem. Soc. 131 (2009) 12868–12869.
[25] D.Z. Li, H.J. Huang, X. Chen, Z.X. Chen, W.J. Li, D. Ye, X.Z. Fu, J. Solid State Chem. 180 (2007) 2630–2634.
[26] P. Periyat, S.C. Pillai, D.E. McCormack, J.C. Colreavy, S.J. Hinder, J. Phys. Chem. C 112 (2008) 7644–7652.
[27] Y.M. Xu, C.H. Langford, Langmuir 17 (2001) 897–902.
[28] J.G. Yu, Y.R. Su, B. Cheng, Adv. Funct. Mater. 17 (2007) 1984–1990.
[29] K.L. Lv, J.G. Yu, K.J. Deng, J. Sun, Y.X. Zhao, D.Y. Du, M. Li, J. Hazard. Mater. 173 (2010) 539–543.
[30] K.L. Lv, J.G. Yu, K.J. Deng, X.H. Li, M. Li, J. Phys. Chem. Solid 71 (2010) 519–522.
[31] M. Liu, K.L. Lv, G.H. Wang, Z.Y. Wang, Y.X. Zhao, Y.R. Deng, Chem. Eng. Technol. 33 (2010) 1531–1536.
[32] M.H. Zhou, J.G. Yu, J. Hazard. Mater. 152 (2008) 1229–1236.
[33] C. Minero, G. Mariella, V. Maurino, E. Pelizzetti, Langmuir 16 (2000) 2632–2641.
[34] M. Mrowetz, E. Selli, Phys. Chem. Chem. Phys. 7 (2005) 1100–1102.
[35] K.L. Lv, J.G. Yu, L.Z. Cui, S.L. Chen, M. Li, J. Alloys Compd. 509 (2011) 4557–4562.
[36] J.C. Yu, J.G. Yu, W.K. Ho, Z.T. Jiang, L.Z. Zhang, Chem. Mater. 14 (2002) 3808–3816.
[37] J.G. Yu, Q.J. Xiang, J.R. Ran, S. Mann, CrystEngComm 12 (2010) 872–879.
[38] K.L. Lv, Y.M. Xu, J. Phys. Chem. B 110 (2006) 6204–6212.
[39] Y.M. Xu, K.L. Lv, Z.G. Xiong, W.H. Leng, W.P. Du, D. Liu, X.J. Xue, J. Phys. Chem. C 111 (2007) 19024–19032.
[40] K.L. Lv, X.F. Li, K.J. Deng, J. Sun, X.H. Li, M. Li, Appl. Catal. B 95 (2010) 383–392.
[41] J.G. Yu, T.T. Ma, S.W. Liu, Phys. Chem. Chem. Phys. 13 (2011) 3491–3501.
[42] M.H. Zhou, J.G. Yu, S.W. Liu, P.C. Zhai, B.B. Huang, Appl. Catal. B 89 (2009) 160–166.